

13 **Abstract**

14 Photogrammetric reanalysis of 1985 aerial photos has revealed substantial submarine
15 melting of the floating ice tongue of Jakobshavn Isbrae, West Greenland. We derived 20-
16 m grid digital elevation models with an elevation uncertainty of ± 2.8 m and used these to
17 assess the thinning of the ice tongue as a function of flow line distance. Feature tracking
18 on orthophotos showed July 1985 ice tongue speeds to be nearly constant from the
19 grounding zone to the terminus (~ 18.5 m d⁻¹). Using ice thickness calculated from
20 hydrostatic equilibrium and assuming negligible dynamic thinning, we determined an
21 area-averaged melt rate of 0.60 m d⁻¹ (220 m a⁻¹) for the main ice stream. We
22 hypothesize that the cause of the high melt rate is the circulation of warm seawater
23 (thermal forcing of up to 4.3 °C) beneath the tongue with convection driven by the
24 substantial discharge of subglacial freshwater from the grounding zone. The terminus
25 and ice stream were in approximate equilibrium from 1964 to 1997. A dramatic thinning,
26 retreat, and speedup began in 1998 and continues today. The timing of the change is
27 coincident with a 1.1 °C warming of deep ocean waters entering the fjord by 1997.
28 Assuming a linear relationship between thermal forcing and submarine melt rate, average
29 melt rates should have increased by $\sim 25\%$ (~ 55 m a⁻¹). We propose that this increase
30 was sufficient to destabilize the ice tongue and initiate the ice thinning and retreat that
31 followed.

32

33 Index terms: Cryosphere, Ice Streams, Ice tongues, Submarine Melting, Dynamics

34

35

36 **1. Introduction**

37 Jakobshavn Isbrae (JI) in West Greenland drains ~ 7 % of the Greenland Ice Sheet
38 (Bindschadler, 1984) and is the largest of the ice sheet's outlet streams (Fig. 1). JI was
39 in approximate equilibrium during the period between 1964 and 1997 with the terminus
40 fluctuating about 1 - 2 km about a seasonally averaged position (Pelto et al., 1989; Sohn
41 et al, 1998; Csatho et al., 2008). Echelmeyer and Harrison (1990) (EH, 1990 hereafter)
42 and Echelmeyer et al. (1991) (ECH, 1991 hereafter) reported ice tongue speeds ~ 18 m d⁻¹
43 for 1985-86 with no seasonal variations. Thinning of the ice tongue began in 1998 and
44 was accompanied by a 1 – 2 km retreat of the terminus (Thomas et al., 2003; Luckman
45 and Murray, 2005). Ice tongue speeds began accelerating between 1998 and 1999,
46 increasing 30 % by 2001 (Thomas et al., 2003; Luckman and Murray, 2005; Joughin et
47 al., 2004). The continued thinning, retreat, and speedup of JI has been documented by
48 numerous subsequent investigations (e.g., Podlech and Weidick, 2004; Krabill et al,
49 2004; Joughin et al., 2004; 2008; Thomas et al., 2008; Amundson et al. 2008; 2009):
50 speeds have more than doubled, the terminus has retreated more than 15 km, and total
51 thinning along the lower reaches of the ice stream has exceeded 200 m. The causes of
52 these rapid and remarkable changes at Jakobshavn have been attributed to a variety of
53 factors including: 1) increased surface melting inland (Zwally et al, 2002), 2) increased
54 (or disequilibrium) bottom melting of the ice tongue (Thomas et al, 2003), and/or 3)
55 changes in ice dynamics associated with force perturbations caused by thinning (Thomas
56 et al., 2004; Joughin et al., 2008).

57

58 In this paper we explore conditions that existed in the terminus region during its recent
59 period of relative stability by examining two sets of high elevation (~13,500 m), high
60 resolution (~2 m) aerial photographs of Jakobshavn Isbrae that were acquired two weeks
61 apart during July 1985 (Fastook et al, 1995). These historic photo sets have become
62 increasingly important for documenting and understanding the dynamic state of this
63 outlet stream prior to the rapid retreat and massive ice loss that began in 1998. The
64 original photogrammetric analysis of this imagery is summarized in Fastook et al. (1995).
65 They derived a coarse Digital Elevation Model (DEM) over an area of approximately 100
66 km x 100 km by interpolation from several hundred positions determined manually from
67 block-aerial triangulation and derived a number of velocity vectors by photogrammetric
68 feature tracking. Prescott et al. (2003) examined the terminus region more intensively
69 and photogrammetrically determined surface elevations and motion vectors for about 500
70 crevasses on the floating ice, and adjacent grounded ice. Based on their analysis of
71 strain rates and ice tongue thickness, they estimated that the bottom melt rate along the
72 base of the floating tongue was at least 109 m a^{-1} .

73

74 We have re-analyzed these photos sets using digital photogrammetry (BAE Socet Set[©])
75 and significantly improved DEM quality and resolution. We were also able to resurvey
76 the original land-based photo control points (which are still visible in the field) with
77 modern GPS survey methods and significantly increased their accuracy. High quality
78 orthophotos were generated using our improved DEMs and then used for automated
79 feature tracking to derive a dense set of velocity vectors for the terminus. In this paper we
80 analyze these new DEMs and orthophotos to specifically assess the degree of submarine

81 melting of the tongue during a period when the ice stream was in an approximately
82 “equilibrium” state. Our analysis shows that substantial submarine melting existed along
83 the floating tongue in 1985, more than twice that estimated by Prescott et al. (2003). By
84 extension, we believe these melt rates existed throughout its period of relative stability
85 (1964 – 1997) and that this melting was a significant factor in controlling ice tongue
86 thickness. We further propose that significant increases in ocean temperature by 1997
87 caused the rate of bottom melting to increase, thereby thinning the ice tongue, and that
88 such changes initiated the destabilization of JI. Evidence for these assertions derives
89 from a seawater temperature time series in Disko Bay and from comparisons of NASA
90 Airborne Thematic Mapping (ATM) profile data of the ice tongue to our DEM.

91

92 **2. Methods, Data, and Uncertainties**

93

94 **2.1 Photogrammetry**

95 The original negatives of the 1985 aerial photos, flown July 10 and July 24, are archived
96 at Mark Hurd Inc. (Minneapolis). We obtained 14 micron scans for our digital
97 photogrammetry analysis. Estimated pixel ground resolution is ~ 2 m. Ground control
98 point (CP) coordinates were surveyed in 1985 by a U. of Maine field party (H. Brecher,
99 written comm., OSU) using Doppler Satellite Radar (DSR). The CP array consisted of 7
100 points on land and 7 points on ice. The land-based markers were still visible during our
101 2007-2009 field campaigns and we resurveyed these points using precision GPS methods.
102 We found horizontal and vertical biases in the original coordinates of ~ -11 m and -4 m
103 respectively. We used our GPS-determined coordinates for the land CPs and applied a

104 transformation to the 1985 ice CP coordinates for our photogrammetric analysis. We
105 estimate the accuracy of the GPS-surveyed land CPs at ± 0.3 m. Brecher (written comm.)
106 estimated the DSR uncertainty for five of the ice CPs at 0.6, 0.9, and 0.7 m for X, Y, and
107 Z respectively. The two remaining ice CPs had significantly higher uncertainties but lie
108 well beyond the terminus, which is our region of interest.

109

110 We optimized photo contrast for glacier visibility and used BAE Socet Set (BAE-SS)
111 digital photogrammetry NGATE software, optimized to perceive the glacier surface, to
112 derive 20-m-grid DEMs of the terminus region from the two sets of aerial photos. The
113 software program automatically weights the CPs according to uncertainty to control the
114 positions and orientations of the photos. The BAE-SS reported RMS model fit was < 1 m.

115

116 We assessed the accuracy of the DEMs using various ground truthing data sets. These
117 data sets are almost exclusively over land and include NASA ATM profiles and our own
118 kinematic and static GPS surveys, performed during field campaigns in 2006 -2009. We
119 used tiled ATM data, filtered for slope roughness and excluded land terrain where we
120 knew the DEM failed to model the land surface. The results of comparing elevations at
121 ~ 9000 points showed a Gaussian distribution with a standard deviation (δ_{sd}) = 2.8 m and
122 a slightly negative bias (-0.7 m). Unfortunately, we lack ground truthing data for the
123 1985 ice surface in the terminus region. However, eight ice positions were surveyed
124 further upstream by DSR in 1985. We adjusted these positions for biases and estimate
125 their accuracy at ± 1 m. Comparison of these elevations (adjusted for ablation losses
126 where needed) to our DEM yielded $\delta_{sd} = 2.4$ m, very similar to our land results. Given

127 these ice results and that the land points lie in close proximity to the ice margins (< 5
128 km), we assigned an elevation uncertainty of ± 2.8 m for the terminus ice surface DEMs.

129

130 **2.2 Velocities**

131 We generated orthophotos based on our DEMs and used the orthophotos for feature
132 tracking and velocity determinations at 100-m grid points, using a modified form of
133 IMCORR (Scambos et al., 1992). The uncertainty of these velocities, based on degree of
134 pixel correlation, is estimated at ± 0.3 m d⁻¹. We generated streamlines from the gridded
135 velocity field using Matlab (TM) streamline function. These stream lines were then
136 used to bound regions of the South Branch (SB) to analyze ice fluxes and submarine melt
137 rates along the floating tongue.

138

139 **2.3 Seawater Data**

140 During the last three decades the Greenland Institute of Natural Resources (GINR) has
141 collected CTD data at a station located in Disko Bay, near the village of Ilulissat and
142 entrance to Kangia Ice Fjord (Fig. 1; $\sim 69.25^\circ$ N, 51.3° W). Casts were made on an
143 annual basis at this station from 1980 to 2008 except for 1991 – 1993 and 1996. For
144 1991 and 1993 we used data from a station about 1 degree further west. There are no
145 data for 1992 and the closest station in 1996 was 4 degrees further west. The date of
146 occupation varied from year to year but was always in summer, between mid June and
147 late August.

148

149 **2.4 Hydrostatic Equilibrium**

150 Our goal here is to determine the bottom topography of the floating tongue using the
151 surface topography of our DEM. We chose the July 24 DEM for this analysis because of
152 its better image definition. The first step is to adjust for voids created by crevasses. The
153 resolution of our 20 m grid is sufficient to capture major crevasses, which are spaced
154 about 100 m apart on the floating tongue and have depths of 20 to 30 m. We applied an
155 equal weight filter with a radius of 0.5 km to produce a smoothed surface. This
156 procedure compensates for the voids created by crevassing, which is important when
157 estimating hydrostatic equilibrium depths. We estimate the uncertainty in void space
158 using this method at ± 1 m freeboard, which is equivalent to about 9 m of ice depth. Note
159 that we ignore any bottom crevassing on the ice tongue.

160

161 Since our photogrammetry uses CPs that are based on an ellipsoid, our next step is to
162 transform surface elevations to mean sea level (msl). We used the EGM96 geoid model
163 for this conversion. These geoid corrections range from 28 to 29 m across our area of
164 interest and are nearly linear. Correction for tidal stage is not necessary as the July 24,
165 1985 photos were flown when tide was at about mean sea level.

166

167 The next step is to calculate hydrostatic equilibrium ice depths from the smoothed surface
168 DEM. This requires assumptions about the density of glacier ice (ρ_i) and seawater (ρ_s).
169 We use 910 kg m^{-3} for the former based on findings of Lüthi et al. (2002) (in upglacier
170 boreholes) and prescribe an uncertainty of $\pm 7 \text{ kg m}^{-3}$ (pure ice to “bubbly” ice). The
171 density of seawater depends primarily on salinity but also on temperature and pressure.
172 As we will discuss later, there is good evidence for circulation of seawater mixed with

173 subglacial freshwater beneath the ice tongue. Summertime CTD data from the GINR
174 oceanographic station near Disko Bay (Fig. 1) indicates that seawater entering the fjord
175 across the entrance sill in 1985 (300 – 350 m deep) had a salinity of $S = 33.5$ and
176 temperature $T = 1.8$ °C (cf. Fig. 7). The pressure melting point for $S = 33.5$ at 800 m
177 depth (approximate depth at the grounding zone) is -2.5 °C, so the thermal forcing is 4.3
178 °C. We assume that subglacial freshwater discharge emerging from the grounding zone
179 mixes with this seawater and that the mixed water forms the buoying medium for the ice
180 tongue. Based on mixing ratios in waters emerging from submarine melting of tidewater
181 glacier termini elsewhere (e.g., Alaska (Motyka et al., 2003); fjords north of Jakobshavn
182 (Rignot et al., in revision); Petermann Glacier (Rignot and Steffen, 2008)), we assume
183 that the mixed water flowing beneath the tongue is at $T \sim 0.5$ °C and has a salinity of $S =$
184 31 . Density ρ_s at this T and S varies from 1026.8 kg m⁻³ at 400 m depth to 1028.7 kg m⁻³
185 at 800 m depth. We used these values in an iterative process to determine seawater
186 densities along the base of the tongue. We then used these densities for our analysis of
187 hydrostatic equilibrium. More dilute (less buoyant) seawater results in greater ice depths,
188 while more saline seawater (more buoyant) decreases the estimated ice depth. For
189 example, a change in salinity of ± 3.5 would change the estimated ice depth by about ± 10
190 m.

191

192 **2.5 ATM Data**

193 We use NASA ATM flights of Jakobshavn Isbrae to assess changes to the ice tongue
194 after 1985. We acquired these data sets from W. Krabill (Pers. Comm., 2008 and 2009) in
195 ICESAT format, and then used the XY flight line coordinates to derive 1985 surface

196 profiles from our DEM. The latter were then compared to ATM elevations to determine
197 changes in surface elevations. Repeat ATM lines were also differenced to assess changes
198 between flights. The first ATM flights over the terminus were conducted in 1993 and
199 approximately followed the SB centerline (cf. Fig. 8). Subsequent flights of SB were
200 over the north edge of the ice stream in 1997, 1998, and 2001 and a cross profile at 546
201 km Easting (UTM zone 22N) in 1997 (cf. Fig. 8). ATM data is also available for a
202 portion of the NB on a nearly annual basis from 1993 to 2001 (cf. Fig. 8) (Thomas et al.,
203 2003).

204

205 We also acquired ATM data for flights that were flown over land adjacent to the terminus
206 floating tongue. These data were used to help assess the accuracy of our photogrammetric
207 DEM, as discussed above. The reported accuracy of the ICESAT ATM data is ± 0.3 m.

208

209 **2.6 Propagation of uncertainties**

210 The principal sources of potential systematic error in our calculation of hydrostatic
211 equilibrium thickness of the floating tongue include uncertainties in ρ_i (± 7 kg m⁻³), ρ_{sw} (\pm
212 2.5 kg m⁻³), DEM model bias (± 0.7 m), Geoid (± 0.5 m), and estimating crevasse void
213 space (± 1 m). In addition, there is a quasi-random uncertainty (cf. Rolstad et al., 2009)
214 in our DEM elevation determinations of ± 2.8 m. From propagation of uncertainties, an
215 ice thickness of ~ 800 m would have an associated uncertainty of ± 50 m. Uncertainty in
216 thickness is dominated by the uncertainty in ρ_i . We view this as a “systematic”
217 uncertainty affecting the absolute values of ice tongue thickness; the relative form of the
218 ice tongue geometry, however, would remain the same.

219

220 **3. Results**

221 **3.1 Topography and Velocity**

222 A shaded relief image with a 50-m interval contour overlay based on the July 24, 1985
223 20-m grid DEM is shown in Fig. 2. The results of the velocity analysis are displayed in
224 Fig.3, overlaid on the orthophoto for July 24. Our speeds are in excellent agreement
225 with ground-based optical surveys of targets on the tongue reported by EH (1990) and
226 ECH (1991) but are slightly faster than previously reported photogrammetric results
227 (Pelto and Hughes, 1989; Fastook et al., 1995). The latter may be a consequence of our
228 much higher resolution DEM, which allows better registration of orthophotos and
229 therefore the terminus velocity field. Streamlines derived from the velocity field are also
230 shown on Fig. 2.

231

232 The 1985 ice flow pattern for the South Branch (SB) shows speed increasing as ice flows
233 into the grounding zone (GZ), reaching a maximum of 19.7 m d^{-1} (Fig. 3b) (see Figs. 2
234 and 4 for location of GZ). Ice speed then slowed to 18.4 m d^{-1} on the ice tongue and was
235 essentially constant for the next 8 km with negligible longitudinal strain rates (Fig. 3b). In
236 the last kilometer before the calving front, speed reached 21.4 m d^{-1} . The dominance of
237 the 1985 SB ice stream is clearly evident in Figs. 2 and 3.

238

239 **3.2 Grounding Zone**

240 We use the term grounding “zone” (GZ) (following arguments of EHC, 1991) and
241 estimate its position to lie between 549.5 km and 550.0 km Easting UTM (Fig. 2) based

242 on several arguments. The average ice thickness of the SB at 549.5 km (discussed later)
243 is $\sim 930 (\pm 50)$ m. This thickness is consistent with measurements made of icebergs
244 related to full-ice-thickness calving events in 2008 (900 ± 50 m, Lüthi et al., 2009) and
245 other calving events that occurred in this general vicinity during 2007 and 2008
246 (Amundson et al., 2008; 2009). This thickness is also consistent with soundings made by
247 Holland et al. (2008) in the proglacial area (cyan dots in Fig. 2), which exceeded 800 m
248 in depth. Bed depths slightly greater than 800 m are also consistent with ice cliff heights
249 determined from our various field surveys during 2007 – 2009. Another indicator of
250 grounding zone position is the change in velocity: SB ice velocity first increases and then
251 decreases in the region around 550 km (Fig. 3). Such changes are consistent with
252 numerical models for changes in speed across a grounding line (Goldberg and Holland, in
253 press; M. Lüthi, pers. comm., 2009). Our position for the GZ differs from Thomas et al.
254 (2003), who placed the GZ ~ 2 km further upstream, and Csatho et al. (2008), with GZ ~ 2
255 km further downstream.

256

257 **3.3 Bottom Topography of the South Branch**

258 Here we focus on the 1985 bottom topography of the SB, which drains the majority of the
259 Jakobshavn Isbrae basin and contributes ~ 80 % of the ice entering the floating tongue.
260 We chose for detailed topographic analysis a ~ 3 -km-wide, 10-km-long section of the SB
261 extending from 541 km to 551 km Easting (10 km) (see Fig. 2 for boundaries). The west
262 boundary for this “ribbon” of floating ice was dictated by the location of the calving
263 zone, which lies ~ 500 m west of 541; the east boundary, by the GZ. Shear zones along
264 the fjord walls pose problems because ice flexure associated with buttressing effects can

265 prevent ice from achieving full hydrostatic equilibrium (Lingle et al., 1981). Our velocity
266 map indicates that the south wall shear zone extends for ~1 km from the south wall
267 grounding line (Fig. 3) and we therefore positioned the south boundary of the ribbon
268 accordingly (~ 1.1 km). This boundary also avoids problems with the topographic
269 feature labeled “Rumple” (ECH, 1991), where we know bedrock is quite shallow and the
270 ice is not in hydrostatic equilibrium. The shear zone on the north side is more
271 complicated and much wider (ranging from 1 - 2 km from the north wall grounding line).
272 We placed the ribbon boundary south of this zone: it roughly coincides with a region
273 called the “zipper” (ECH; 1991), which is the juncture of ice flow from the two main
274 branches (Fig. 2). Our choices are in accord with field measurements by Lingle et al.
275 (1981), which indicated that the floating tongue was fully responsive to tidal flexure at
276 distances of about 1 – 1.5 km or more from the north wall. Our choice of boundaries also
277 avoids other ice margin problems associated with our smoothing of the surface terrain.
278
279 Figure 4 displays the SB bottom topography based on the assumption of hydrostatic
280 equilibrium, using our smoothed surface DEM. Our choice of a “smoothing” distance
281 was a compromise: it needed to be long enough to smooth out crevasse fields but also
282 short enough not to average out interesting bottom features. Small bottom features cannot
283 be resolved, because they are not expressed at the surface, but larger features manifest
284 themselves in the surface elevations in a “smoothed” or “blurred” manner (Rignot and
285 Steffen, 2008). Despite the qualitative nature of Fig. 4, our analysis reveals the existence
286 of a large “channel” incised into the bottom of the ice tongue. This channel emanates
287 from the deepest part of the grounding zone, in the center of the SB, and continues to the

288 terminus along the center flowline. The smoothing process has likely made the channel
289 appear wider and shallower than it is in actuality. There is also a "natural filter" at work
290 here, i.e., a narrow deep channel would not reveal itself as such on the surface given the
291 thickness of ice. Nevertheless, we can reasonably state that the channel is at least a
292 couple of 100 m in width and several tens of m in depth.

293

294 **3.4 Flux Gates and Submarine melting**

295 Knowing the ice thickness and velocity field of the ice tongue allows us to calculate ice
296 fluxes through flux gates and thus evaluate the amount of submarine melting occurring
297 along the SB ice tongue shown in Fig. 4. We assume that velocity did not vary
298 seasonally during the mid-1980's (cf. EH, 1990) and, based on the stability of the
299 terminus position from 1964 – 1997, we assume an approximately steady-state ice
300 thickness profile. We conservatively place the entrance gate at 549.5 km easting, a
301 position where we are confident that the ice is in hydrostatic equilibrium. The exit gate is
302 at 541.5 km easting, to avoid complications with flexure as ice approaches the calving
303 front and accelerates (Fig. 2). We used streamlines to define our north and south
304 boundaries so that no ice flux occurs across the lateral boundaries. The net ice loss
305 between the gates was then computed. An adjustment was made for surface ablation
306 losses of $\sim 4 \text{ m a}^{-1}$ (ice equivalent) on the tongue (Echelmeyer et al., 1992) and the
307 remainder we attribute to submarine melting. The area-averaged results for the SB flow
308 band are reported in Table 1. (Note that if the ice was in hydrostatic equilibrium at 550.0
309 km easting and we chose this as the entrance flux gate, the area-averaged estimated melt

310 rate would be $\sim 50 \text{ m a}^{-1}$ higher.) Calving, submarine melting, and surface ablation
 311 account for roughly 70, 29, and 1 % of ice losses from the SB floating tongue in 1985.

312

313 Table 1. Ice losses between flux gates and
 314 area-averaged melt rates.

	“South Branch”
Net ice loss, $\text{km}^3 \text{ a}^{-1}$	5.09 ± 0.30
Ablation, $\text{km}^3 \text{ a}^{-1}$	0.09 ± 0.01
Submarine melt rate, $\text{km}^3 \text{ a}^{-1}$	5.00 ± 0.30
Area average melt rate, m a^{-1}	220 ± 14
Area average melt rate, m d^{-1}	0.60 ± 0.04

315

316 To obtain more detailed information on the distribution of submarine melting along the
 317 SB flow band bounded by the streamlines, we present submarine melting in two ways. In
 318 the first case, we calculated the width averaged melt rates by analyzing ice flux through \sim
 319 3-km wide (perpendicular to flow) gates at every 250 m along-flow interval. To smooth
 320 out noise, we used a 0.5-km along-flow sliding window (0.5 km is the radius of our initial
 321 smoothing of surface topography). The resulting area-averaged submarine melt rates are
 322 plotted in Fig. 5 along with the width-averaged cross-sectional ice thickness. The melt
 323 signal is primarily driven by slopes from our calculated bed topography and is highest
 324 just downstream of the GZ: $1.5 - 1.8 \text{ m d}^{-1}$ ($550 - 670 \text{ m a}^{-1}$). Melt rates gradually
 325 decrease until they are no longer detectable between $545.25 - 545.25 \text{ km}$ easting, where
 326 velocities and ice thickness are both constant. Melt rates along the remainder of the
 327 tongue range between $0.15 - 0.50 \text{ m d}^{-1}$ ($55 - 180 \text{ m a}^{-1}$).

328

329 We also calculated melt rates by averaging ten grid points (100 m spacing) perpendicular
330 to flow along a set of narrower flow bands within the larger flow band. Fig. 6 provides
331 this more detailed melt signal information and shows the values that are being averaged
332 together in the 3 km wide flow band analysis. Details much less than 0.5 km are lost
333 because of the smoothing process used in constructing bottom topography. The mottled
334 pattern is interesting and indicates that the distribution of submarine melting is complex.
335 There is a "cold spot" right at the center of the grounding zone, perhaps an indicator of
336 upwelling of cold freshwater discharge or irregularities in the grounding zone. The cold
337 spot is followed by a "warm spot", a region where we might expect turbulent mixing with
338 warm ocean waters to be strongest. There are also two "warm spots" along the south
339 edge of the flow band; one is adjacent to the "Rumple". We are uncertain how to
340 interpret these spots but they may be related to thicker ice to the south caused by
341 buttressing effects. The thicker ice could cause the bottom to reach warmer water.

342

343 **3.5 Seawater Data**

344 Figure 7 displays the temperature data obtained from the GINR CTD casts at Station 26
345 (Fig. 1). We also included data for 1991 and 1993 from a station 1° further west to fill in
346 the data gap. (Data for the uppermost part of the water column in 1993 – 1995 are erratic
347 and appear to reflect local circulation effects; we therefore did not include them in Fig.
348 7.) The deepest and warmest water (at 300 - 350 m) averaged 1.7 °C during the 1980s.
349 Despite data gaps, there appears to have been a distinct cooling trend during the mid-90s.
350 The record then shows that a significant and sustained increase in seawater temperature
351 occurred at all depths by 1997. Temperatures of deep water (300 – 350 m) averaged 2.8

352 °C between 1997 and 2008, an increase of 1.1 °C with respect to the 1980s decade. In
353 contrast, salinity did not show any significant change between 1980 and 2008.

354

355 **3.6 Post-1985 surface elevation changes**

356 Comparisons of 1985 DEM and ATM surface profiles (see Fig. 8 for location of profile
357 lines) and elevation changes are shown in Figures 9 – 12. These profiles are mostly over
358 floating portions of the terminus, thus it is important to bear in mind that slight changes
359 in surface elevation can reflect significant changes in overall ice thickness.

360

361 Of the ATM lines available prior to the dramatic changes that started in 1998, only one
362 was flown over the SB (line SB flown on 09-July-93; Fig. 8). Comparison of line SB to
363 the 24-July-85 surface reveals little change along most of the path, indicating the
364 terminus remained in a state of approximate equilibrium (Fig. 9). Some changes are
365 evident both near the terminus and over the GZ. These changes reflect a slight advance
366 of the terminus and perhaps also the grounding zone. Both of these differences could be
367 attributed in part to the fact that the ATM profile was flown 2 weeks earlier in the
368 summer than our July 24, 1985 DEM, and thus may be seasonal effects.

369

370 Gradual increase in the elevation of ice on either side of the SB between 1985 and 1997
371 is evident in the transverse profile that transects the tongue at 546 km easting, about half
372 way between the GZ and the terminus (line T in Fig. 8) as shown in Fig. 10. This
373 increase occurs over regions that are known to be grounded or over a shear zone margin,
374 the latter of which is quite wide (~ 2 km) on the north end of this transect. As discussed

375 before, changes in the shear zones may not be readily amenable to interpretation in terms
376 of hydrostatic equilibrium because of buttressing effects. However, what is interesting is
377 that ice elevation did not change significantly over the central part of the SB ice stream,
378 the flow band where we believe ice to be in hydrostatic equilibrium and where we
379 performed our analysis of melting for Figs. 5 and 6. The lack of significant changes
380 indicates that the melt channel continued to be very active into 1997.

381

382 Line NB, which crosses a section of the NB floating tongue (Fig. 8), had the greatest
383 frequency of flights during the 1990s and changes that occurred along this flight line have
384 been reported by Thomas et. al. (2003) and Csatho et al. (2008). Here, we focus on the
385 tongue and terminus portion of the flight line (Fig. 11). Ice elevations on this section
386 gradually increased by a few meters during the first part of the 1990's but then dropped
387 by $\sim 6 \text{ m a}^{-1}$ between 1997 and 1998 with the rate of surface change increasing to $\sim 10 \text{ m}$
388 a^{-1} in succeeding years.

389

390

391 We next examine an ATM path flown on 13-May-97, then again on three separate days
392 (June 29, July 13 and July 15) in 1998 over the east part of the SB, the “Zipper”, and up a
393 steep ridge (Line Z in Fig. 8) (elevation changes shown in Fig. 12). Terminus
394 fluctuations are clearly evident with an advance of $\sim 2 \text{ km}$ between 1985 and 1997
395 followed by an abrupt retreat of over 4 km during 1997-98. The 1985 – 1997 advance
396 may be partly attributable to the 2 month seasonal difference. However, the ice surface
397 also rose at a rate of $\sim 2 \text{ m a}^{-1}$ in the region between 545 km easting and the base of the

398 steep ridge. In contrast, the surface generally dropped at rates of up to 5 m a^{-1} between
399 1997 and 1998. An ATM line was flown on 27-May-01 (line Z' in Fig. 8) but it is not
400 directly comparable to 1997 and 1998 because the path lies about 300 m north of line Z.
401 However, a comparison to the 1985 DEM surface is shown in Fig. 12 (dashed lines). To
402 derive an approximate rate of change in surface elevation between 1998 and 2001, we
403 assumed that the ice surface in 1998 was at least as high as in 1985. (This assumption is
404 based on a comparison of 1998 to 1985 profiles along the neighboring flight path Z.) The
405 average change between 1998 and 2001 from Fig. 12 is ~ -5 to -6 m a^{-1} ; we consider
406 these rates to be minimum estimates as the 1998 surface is likely to have been somewhat
407 higher than our assumption.

408

409 **4. Discussion**

410 **4.1 Causes of Submarine Melting**

411 The submarine melt rates are surprisingly high. We believe that the direct cause of these
412 high rates of melting at JI is the circulation of warm seawater that is brought into contact
413 with the bottom of the ice tongue through convection driven by subglacial freshwater
414 discharge from the grounding zone (Fig. 4), similar to convection-driven submarine
415 melting of tidewater glaciers in Alaska (cf. Motyka et al., 2003). We also propose that
416 the channel shown in Fig. 4 has been incised into the ice by bottom melting caused by
417 this circulation. The channel location at the deepest and central part of the grounding
418 zone is consistent with the exit of a large subglacial stream from the grounding zone. In
419 addition, Pelto et al. (1989) and EH (1990) both reported regions of strong upwelling of

420 turbid water along the terminus at approximately the same location where our analysis
421 indicates that the channel exits at the terminus.

422

423 Based on an analysis of surface melting and frictional and geothermal melting at the base,
424 EH (1990) estimated the subglacial freshwater discharge at the GZ to be $750 - 1500 \text{ m}^3 \text{ s}^{-1}$
425 ¹ in summer and $64 - 105 \text{ m}^3 \text{ s}^{-1}$ in winter. We believe that the magnitude of this
426 discharge coupled with thermal forcing of $4.3 \text{ }^\circ\text{C}$ at the grounding zone combined to
427 produce the observed high rates of melting. The circulation along the base of the ice
428 tongue is driven by buoyancy. Strongest melting would occur during the summer when
429 discharge-driven convection would be greatest. A decline in thermal forcing also occurs
430 as the mixed water ascends in elevation, resulting in a corresponding decline in melt rate
431 (Fig. 5).

432

433 Figs. 5 and 6 display a curious 1-km-long region of little or no melting that lies between
434 545 and 546 km (easting), about 3.5 km downstream from the GZ. We suspect that this
435 minimum and also the higher melt rates seen further downstream are related to the
436 advection of ice through the GZ during winter and summer regimes. The location of
437 these features at ~ 3.5 and 7 km from the GZ corresponds well with the average speed of
438 the tongue of 6.74 km a^{-1} . The 1 km long stretch of low melting rates corresponds to ice
439 that traversed the GZ ~ 6 months prior to the date of the DEM, in the middle of winter.
440 The higher basal slopes at ~ 7 km from the GZ would have traversed the zone of high
441 melting in the summer of 1984.

442

443 Rignot and Steffen (2008) found submarine melting rates of up to 25 m a^{-1} beneath the 60
444 km long ice tongue of the Petermann Glacier in NW Greenland, an order of magnitude
445 less than found for JI in our analysis. Reasons that may explain this difference in melt
446 rates include: 1) thermal forcing at JI is nearly double that of Petermann; 2) surface
447 ablation is substantially higher (4 m a^{-1} vs 1.2 m a^{-1}); and 3) the JI drainage basin is
448 considerably larger. Both 2) and 3) are expected to lead to more vigorous convection and
449 hence higher rates of heat transfer to the ice. Using radio echo sounding (RES), Rignot
450 and Steffen (2008) also detected substantial meltwater channels incised into the bottom of
451 the floating tongue, similar but better defined than the channel we inferred at JI from our
452 hydrostatic equilibrium analysis.

453

454 Our rates are also twice as large as estimated by Prescott et al. (2003). We believe the
455 reasons for this difference are related to our much better controlled and defined DEMs,
456 orthophotos, and velocity fields plus our much more thorough analysis of hydrostatic
457 equilibrium and dynamic thinning. Prescott et al. (2003) also showed the problems
458 involved in calculating strain rates in this zone of severe crevassing. Our method of using
459 flux gates (essentially the integrated form of the mass continuity equation) avoids such
460 problems.

461

462 **4.2 Triggering of Current Instability**

463 Our analysis of melt rates is based on conditions that existed in 1985. We believe that
464 these melt rates and the overall thickness geometry of the floating tongue are probably
465 representative of the Jakobshavn system between 1964 - 1997. These assertions are

466 based on the following factors: 1) the terminus remained in a relatively stable position
467 from 1964 to 1997 (Sohn et al., 1998); 2) the velocity on the floating tongue remained
468 essentially constant from 1961 to at least 1986 (Pelto et al., 1989); and 3) seawater
469 temperatures at station 26, although showing some oscillation, showed no significant
470 long term change during 1980 - 1990. This quasi-equilibrium status appears to have
471 extended into 1993 based on the similarity of the 1993 tongue surface profile to 1985
472 (Fig. 9). However, some thickening did take place at the GZ, coincident with an apparent
473 decline in tongue velocity to $\sim 16 \text{ m d}^{-1}$ (Joughin et al., 2004). Velocities remained at this
474 value, or remained near constant into 1998 (Joughin et al., 2004; Luckman and Murray,
475 2005) with minor thickening continuing into 1997. The cause of this thickening and
476 velocity perturbation is likely related to either increased glacier surface mass balance
477 and/or a decline in bottom melting of the tongue. There is insufficient mass balance data
478 to assess the former. However, there is evidence for the latter. Although there are gaps
479 in the seawater temperature record for the period 1991 – 1996 at Station 26, inclusion of
480 data from the station further west indicates that there was a decline in deep seawater
481 temperatures during the mid-1990's, perhaps by as much as $0.5 \text{ }^{\circ}\text{C}$ or more. This drop in
482 temperature would have decreased the degree of thermal forcing, thereby reducing the
483 bottom melt rate. This reduction in turn would allow thickening of the floating tongue,
484 causing the observed perturbation.

485

486 A major destabilization of the terminus was clearly initiated during the summer of 1998,
487 as evidenced by glacier thinning, retreat, and speed up (Thomas, 2004; Joughin et al.,
488 2004; Luckman and Murray, 2005). This destabilization progressively increased in

489 magnitude during the following years and continues today. Here, we discuss what we
490 believe to be the probable trigger for these dramatic changes. Given that submarine
491 melting accounted for ~ 29 % of ice loss along the SB floating tongue during its recent
492 “equilibrium” phase, it is reasonable to assume that any significant change in seawater
493 temperature and/or meltwater discharge would correspondingly affect the ice balance of
494 the floating tongue. The GINR CTD station near the mouth of the Kangia Ice Fjord
495 allows us to evaluate the former. Although there are some gaps in the data, the record
496 does convincingly show that a significant and sustained increase in seawater temperature
497 took place after 1997 (Fig. 7). Holland et al. (2008) argued that an upwelling of deep
498 warm ocean waters associated with the North Atlantic Irminger Current recently migrated
499 up the west coast of Greenland, reaching Disko Bay by 1997 and they hypothesized that
500 this current was the cause of the observed increase in seawater temperature. They also
501 proposed that the increase in ocean temperature affected the deep waters entering Kangia
502 Ice Fjord and may have been at least partially responsible for triggering the collapse of JI
503 that began in 1998.

504

505 The depth of the entrance sill into the fjord is 350 m (Holland et al., 2008). We assume
506 that the circulation pattern in the fjord forces deep waters to cross the sill and continue up
507 the fjord. If we use the increase in seawater temperatures of ~ 1.1 °C for bottom waters
508 (Fig. 7) and assume a simple linear relationship between thermal forcing and submarine
509 melt rate (justified on the grounds that subglacial meltwater discharge is the primary
510 force driving convection (cf. P. Holland et al., 2008)), then melt rates should have
511 increased by ~ 25% after 1997 with respect to our derived 1985 melt rates. Applying this

512 change to our area-average melt rate of $\sim 220 \pm 14 \text{ m a}^{-1}$ gives an increased
513 (disequilibrium) melt rate of $\sim 55 \pm 4 \text{ m a}^{-1}$ for the SB, which we believe would be
514 sufficient to destabilize the terminus.
515
516 Although NASA ATM flights over the Jakobshavn floating tongue are sparse for the
517 1990's, they nevertheless do provide evidence for thinning rates that are in accord with
518 our estimates of disequilibrium melting. The equivalent change in freeboard for a
519 disequilibrium melt rate increase of 55 m a^{-1} would be $\sim 5.5 \text{ m a}^{-1}$, rates that are readily
520 detectable from repeat ATM flights. Flight line NB had the highest frequency of flights
521 but crosses just a portion of the floating tongue. The assumption of hydrostatic
522 equilibrium is most reliable for the section from 541 to 545 km easting, before the flight
523 line enters the shear zone and grounded ice (cf. Fig. 2; labeled "floating" in Fig. 11). The
524 change in freeboard for this section averaged $\sim -5.5 \text{ m a}^{-1}$ during 1997 -1998 then
525 increased to $\sim -10 \text{ m a}^{-1}$ during 1998 – 2001. These values compare well, within the
526 uncertainty limits, with the expected average change in freeboard, although the rate of
527 thinning after 1998 may have been influenced by acceleration and dynamic thinning.
528
529 We next examine ATM lines Z and Z' (Fig. 12). These paths traversed the leading edge
530 of the SB then continued over the "Zipper" juncture (cf. Fig. 8). For the period 1997 -
531 1998, the change in freeboard varies considerably along line Z but is most pronounced
532 near the terminus, where it is $\sim -5 \text{ m a}^{-1}$, again similar to the rate expected from our linear
533 assumption. There is little or no change in freeboard along the central part of this path.
534 We note from Fig. 5, that this section of the SB floating tongue experienced the lowest

535 rates of melting and the lack of significant change between 1997 – 1998 may be a
536 reflection of this anomaly. The change in freeboard was again $\sim -5 \text{ m a}^{-1}$ further
537 upstream as the flight line approached the ridge between the south and north branches.

538

539 The change in freeboard ranged between ~ -5 and -8 m a^{-1} between 1998 and 2001, along
540 line Z', again in line with our expectations from increased melting. Actual change may
541 have been higher, given our conservative assumptions on the 1998 ice surface as
542 discussed above.

543

544 Based on this evidence, we believe that the increased disequilibrium submarine melting
545 of $\sim 55 \text{ m a}^{-1}$ was the initial trigger that destabilized the floating tongue. As the tongue
546 thinned, it continued to lose its mooring on stabilizing features. Upstream, the SB
547 progressively accelerated, by 30 % between 1998 and 2001, leading to increased dynamic
548 thinning of ice entering the fjord tongue. This combination of melting and dynamic
549 thinning eventually caused the total disintegration of the floating tongue and led to the
550 glacier's current status.

551

552 The period of retreat and acceleration coincided with a gradual and slight increase in air
553 temperatures and positive degrees days (Thomas, 2004; Csatho et al., 2008; Holland et
554 al., 2008) and an upward migration of the melt zone on the Greenland Ice Sheet (Steffen
555 et al., 2004; Hall et al, 2007). These higher temperatures and increased surface melting
556 would have led to higher rates of subglacial discharge, which in turn would enhance
557 submarine convection and help drive the melting of the floating tongue. They were not

558 the cause of the initial destabilization, as was pointed out by Joughin et al. (2008) at
559 Jakobshavn Isbrae and by Nick et al. (2009) at Helheim Glacier (East Greenland).

560

561 **Conclusions**

562

563 The bottom topography of the July 1985 floating tongue was assessed using high-
564 resolution DEMs and assuming hydrostatic equilibrium. We used values for ice and
565 seawater densities and other parameters that are in good agreement with upstream
566 borehole studies and Disko Bay CTD data. The resultant topography shows a
567 conspicuous channel incised into the bottom of the floating tongue that we believe to be
568 the result of convection-driven melting. Our conservative estimate for the position of the
569 1985 grounding zone is between 594.5 – 550.0 km easting UTM.

570

571 Velocities derived from orthophotos in conjunction with ice thickness allowed estimates
572 of melt rates using ice fluxes. Velocities were essentially constant over most of the 10-
573 km-long 1985 floating tongue and dynamic thinning was negligible except near the
574 terminus. The melt signal is therefore primarily driven by slopes from our calculated bed
575 topography and is highest just downstream of the GZ: $1.5 - 1.8 \text{ m d}^{-1}$ ($550 - 670 \text{ m a}^{-1}$).
576 The area-averaged melt rate is 0.60 m d^{-1} (220 m a^{-1}).

577

578 We believe that the direct cause of these high rates of melting is the circulation of warm
579 seawater that is brought into contact with the bottom of the ice tongue through convection
580 driven by subglacial freshwater discharge from the grounding zone. Given the relative

581 stability of both the terminus between 1964 and 1997 and deep seawater temperatures
582 between 1980 and 1990, bottom melt rates were probably relatively constant during this
583 period. Using a simple linear relationship, we propose that a 1.1°C increase in seawater
584 temperature that occurred by 1997 caused the melt rate to increase by $\sim 55 \text{ m a}^{-1}$.
585 Changes in freeboard determined from post-1997 repeat NASA ATM flights are in good
586 agreement with our estimate of disequilibrium melting. We therefore assert that the
587 direct cause of destabilization of the floating tongue was the significant increase in
588 bottom melting due to an increase in seawater temperature.

589

590 In summary, our photogrammetric analysis shows that Jakobshavn Isbrae's floating
591 tongue was subject to large submarine melt rates well before its recent retreat. A
592 subsequent increase in ocean temperatures, caused by an incursion of warm and saline
593 water (Holland et al., 2008) appears to have thinned the floating tongue to below a
594 critical threshold and led to its disintegration and a dramatic increase in ice flow
595 velocities, confirming conclusions by Thomas et al. (2003). Outlet glaciers in contact
596 with seawater can therefore react very strongly and rapidly to changes in ocean
597 conditions, confirming conclusions by Motyka et al. (2003) in Southeast Alaska.
598 Understanding and predicting rapid glacier changes requires a careful study and
599 monitoring of proglacial fjords and a better understanding of ice-ocean interaction.

600

601 **Acknowledgements**

602

603 H. Brecher generously provided us with his survey data for photo control points and data
604 from his original photogrammetric models. We thank M. Lüthi, J. Amundson, D.
605 Podrasky, and J. Brown for assistance with field work and helpful discussions. I. Howat
606 provided us with a preliminary version of the terminus velocity field using our
607 orthophotos. The SPOT5 image used for the 2007 terminus position was provided by the
608 SPIRIT Program. Funding was provided by NASA's Cryospheric Sciences Program
609 (Grants NNG06GB49G and NNG06GA44G) and the Danish Agency for Science,
610 Technology and Innovation. Additional support was provided by the Geophysical
611 Institute, University of Alaska and the Greenland Institute of Natural Resources.

612

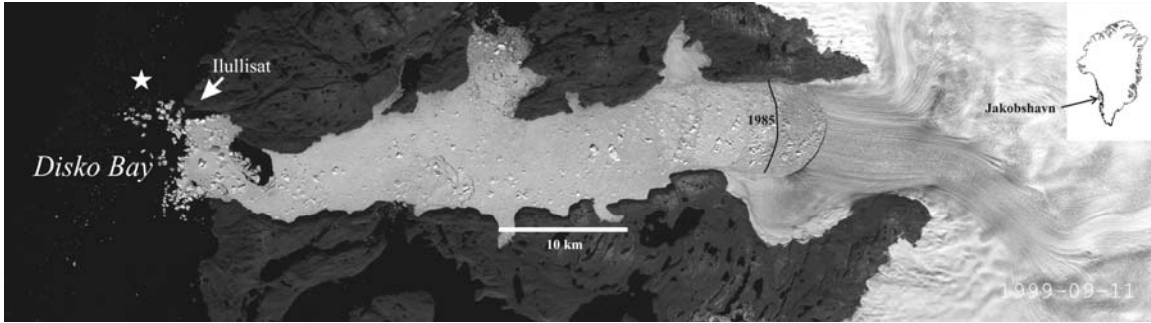
613 **References**

- 614 Amundson, J.M, M. Truffer, M.P. Lüthi, M. Fahnestock, M. West, and R.J. Motyka
615 (2008), Glacier, fjord, and seismic response to recent large calving events,
616 Jakobshavn Isbrae, Greenland, *Geophys. Res. Lett.*, 35(L22501),
617 doi:10.1029/2008GL035281.
- 618 Amundson, J.M., M. Fahnestock, M. Truffer, J. Brown, M.P. Lüthi, and R.J. Motyka (
619 2009), Ice mélange dynamics and implications for terminus stability, Jakobshavn
620 Isbrae, Greenland, *J. Geophys. Res.*, doi:10.1029/2009jf001405, in press.
- 621 Bindschadler, R.A. (1984), Jakobshavns Glacier drainage basin: a balance assessment, *J.*
622 *Geophys. Res.*, **89**(C2), 2066-2072.
- 623 Csatho, B., T. Schenk, C.J. Van der Veen, and W.B. Krabill (2008), Intermittent thinning
624 of Jakobshavn Isbræ, West Greenland, since the Little Ice Age, *J. Glaciol.*,
625 54(184), 131–144.
- 626 Echelmeyer, K. and W.D. Harrison (1990), Jakobshavns Isbræ, West Greenland:
627 Seasonal variations in velocity — or lack thereof, *J. Glaciol.*, 36(122), 82–88.

- 628 Echelmeyer, K., T. S. Clarke and W.D. Harrison (1991), Surficial glaciology of
629 Jakobshavns Isbrae, West Greenland: Part I. Surface morphology, *J. Glaciol.*,
630 37(127), 368-382.
- 631 Echelmeyer, K., W.D. Harrison, T.S. Clarke, and C. Benson (1992), Surficial glaciology
632 of Jakobshavns Isbræ, West Greenland: Part II. Ablation, accumulation and
633 temperature, *J. Glaciol.*, 38(128), 169–181.
- 634 Fastook, J.L., H.H. Brecher and T. J. Hughes (1995), Derived bedrock elevations, strain
635 rates and stresses from measured surface elevations and velocities: Jakobshavns
636 Isbrae, Greenland, *J. Glaciol.*, 41(137), 161-173.
- 637 Goldberg, D. N., D. Holland, and C. G. Schoof (2009), Grounding line movement and ice
638 shelf buttressing in marine ice sheets, *J. Geophys. Res.*,
639 doi:10.1029/2008JF001227, in press.
- 640 Hall, D. K., Williams, R. S., Luthcke, S. B., Digirolamo, N. E. (2008), Greenland ice
641 sheet surface temperature, melt and mass loss: 2000-06, *J. Glaciol.*, 54(184), 81-
642 93, DOI: 10.3189/002214308784409170.
- 643 Holland, D.M., R.H. Thomas, B. DeYoung, M.H. Ribergaard, and B. Lyberth (2008),
644 Acceleration of Jakobshavn Isbræ triggered by warm subsurface ocean waters,
645 *Nature Geoscience*, 1, 659–664, doi:10.1038/ngeo316.
- 646 Holland, P.R., A. Jenkins, and Holland, D.M. (2008) The response of ice shelf basal
647 melting to variations in ocean temperature, *J. Climate*. 21. DOI:
648 10.1175/2007JCLI1909.1
- 649 Joughin, I., I.M. Howat, M. Fahnestock, B. Smith, W. Krabill, R.B. Alley, H. Stern, and
650 M. Truffer (2008), Continued evolution of Jakobshavn Isbræ following its rapid
651 speedup, *J. Geophys. Res. - Earth Surface*, 113(F04006),
652 doi:10.1029/2008JF001023.
- 653 Joughin, I., W. Abdalati, and M. Fahnestock (2004), Large fluctuations in speed on
654 Greenland's Jakobshavn Isbræ glacier, *Nature*, 432, 608–610.
- 655 K. Steffen, S. V. Nghiem, R. Huff, and G. Neumann (2004), The melt anomaly of 2002
656 on the Greenland Ice Sheet from active and passive microwave satellite
657 observations, *Geophys. Res. Lett.*, 31(L20402), doi:10.1029/2004GL020444.

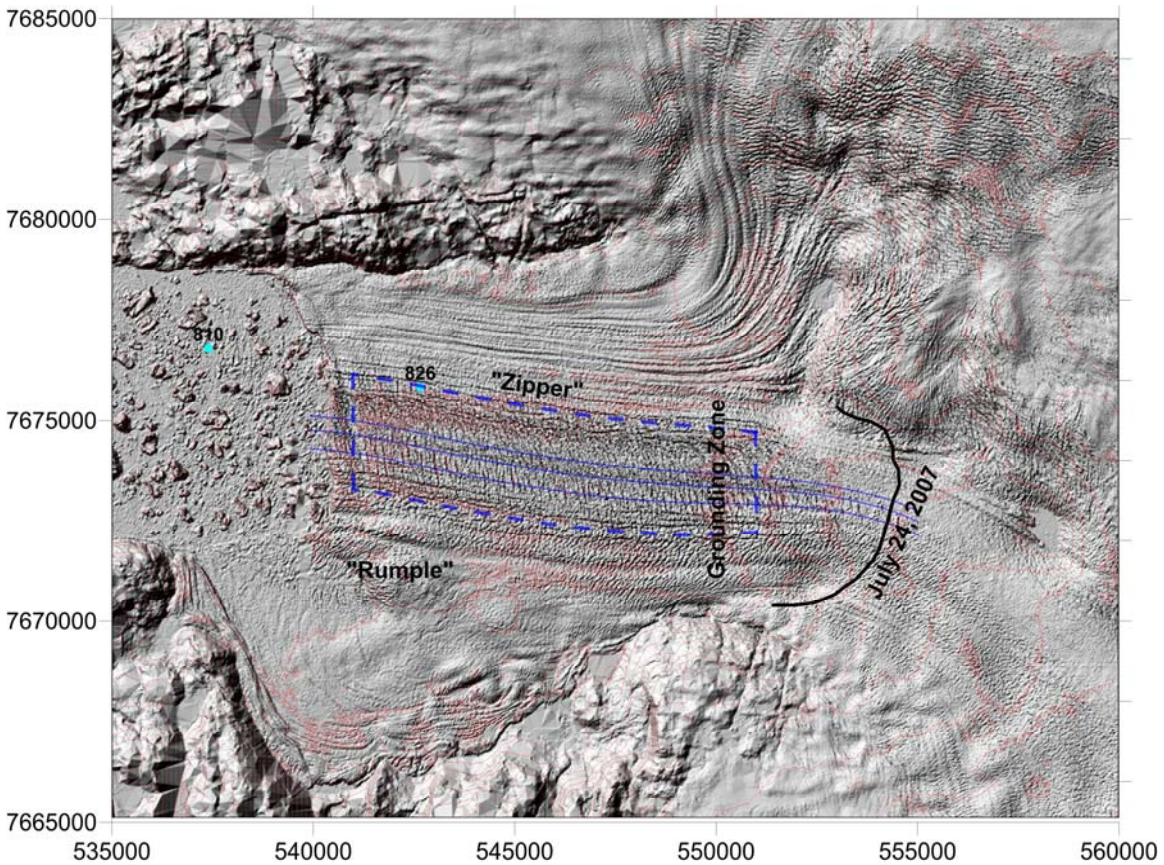
- 658 Krabill, W., E. Hanna, P. Huybrechts, W. Abdalati, J. Cappelen, B. Csatho, E. Frederick,
659 S. Manizade, C. Martin, J. Sonntag, R. Swift, R. Thomas, and J. Yungel (2004),
660 Greenland Ice Sheet: Increased coastal thinning, *Geophys. Res. Lett.*, 31(L24402),
661 doi:10.1029/2004GL021533.
- 662 Lingle, C. S., T. J. Hughes and R.C. Kollmeyer (1981), Tidal flexure of Jakobshavn's
663 glacier, West Greenland, *J. Geophys. Res.*, 86(B5), 3960-3968.
- 664 Luckman, A., and T. Murray (2005), Seasonal variation in velocity before retreat of
665 Jakobshavn Isbrae, Greenland, *Geophys. Res. Lett.*, 32(L08501),
666 doi:10.1029/2005GL022519.
- 667 Lüthi, M., M. Funk, A. Iken, S. Gogineni, and M. Truffer (2002), Mechanisms of fast
668 flow in Jakobshavn Isbrae, west Greenland: Part III. Measurements of ice
669 deformation, temperature and cross-borehole conductivity in boreholes to the
670 bedrock, *J. Glaciol.*, 48(162), 369 – 385, doi:10.3189/172756502781831322.
- 671 Lüthi, M.P., M. Fahnestock, and M. Truffer (2009), Calving icebergs indicate a thick
672 layer of temperate ice at the base of Jakobshavn Isbræ, Greenland, *J. Glaciol.*,
673 55(191), 563-566.
- 674 Motyka, R.J., L. Hunter, K.A. Echelmeyer, and C. Connor (2003), Submarine melting at
675 the terminus of a temperate tidewater glacier, LeConte Glacier, Alaska, U.S.A.,
676 *Ann. Glaciol.*, 36, 57–65.
- 677 Nick, F.M., A. Vieli, I.M. Howat, and I. Joughin (2009), Large-scale changes in
678 Greenland outlet glacier dynamics triggered at the terminus, *Nature Geoscience*,
679 doi:10.1038/NGEO394.
- 680 Pelto, M. S., T. J. Hughes and H.H. Brecher (1989), Equilibrium state of Jakobshavn's
681 Isbrae, West Greenland, *Ann. Glaciol.*, 12, 127-131.
- 682 Podlech, S. and A. Weidick (2004), A catastrophic break-up of the front of Jakobshavn
683 Isbræ, West Greenland, 2002/2003, *J. Glaciol.*, 50(168), 153–154.
- 684 Prescott, P.R., J. P. Kenneally, T. J. Hughes (2003), Relating crevassing to non-linear
685 strain in the floating part of Jakobshavn Isbrae, West Greenland, *Ann. Glaciol.* 36,
686 149 – 156.
- 687 Rignot, E. and P. Kanagaratnam (2006), Changes in the velocity structure of the Green-
688 land Ice Sheet, *Science*, 311(5763), 986–990, doi:10.1126/science.1121381.

- 689 Rignot, E., and K. Steffen (2008), Channelized bottom melting and stability of floating
690 ice shelves, *Geophys. Res. Lett.*, 35(L02503), doi:10.1029/2007GL031765.
- 691 Rignot, E., M. Koppes, I. Velicogna (In Revision), Rapid submarine melting of the
692 calving faces of west Greenland glaciers, *Nature Geosc.*, Manuscript NGS-2009-
693 04-00365B.
- 694 Rolstad, C., T. Haug, B. Denby, 2009, Spatially integrated geodetic glacier mass balance
695 and its uncertainty based on geostatistical analysis: application to the western
696 Svartisen ice cap, Norway, *J. Glaciol.*, 55(192), 666-680.
- 697 Scambos, T, M J Dutkiewicz, J C Wilson and R A Bindshadler (1992), Application of
698 image cross-correlation to the measurement of glacier velocity using satellite
699 remote sensing, *Rem. Sens. Env.*, 42, 177-188.
- 700 Sohn, H.G., K.C. Jezek, and C.J. van der Veen (1998), Jakobshavn Glacier, West Green-
701 land: 30 years of spaceborne observations, *Geophys. Res. Lett.*, 25(14), 2699–
702 2702.
- 703 Thomas, R. H., W. Abdalati, E. Frederick, W. B. Krabill, S. Manizade, and K. Steffen
704 (2003), Investigation of surface melting and dynamic thinning on Jakobshavn
705 Isbrae, Greenland, *J. Glaciol.*, 49(165), 231 – 239,
706 doi:10.3189/172756503781830764.
- 707 Thomas, R.H. (2004), Force-perturbation analysis of recent thinning and acceleration of
708 Jakobshavn Isbræ, Greenland, *J. Glaciol.*, 50(168), 57–66.
- 709 Zwally, H. J., W. Abdalati, T. Herring, K. Larson, J. Saba, and K. Steffen (2002), Surface
710 melt-induced acceleration of Greenland Ice Sheet flow, *Science*, 297(5579), 218–
711 222, doi:10.1126/science.1072708.
- 712
- 713



714
715
716
717
718
719
720
721
722
723

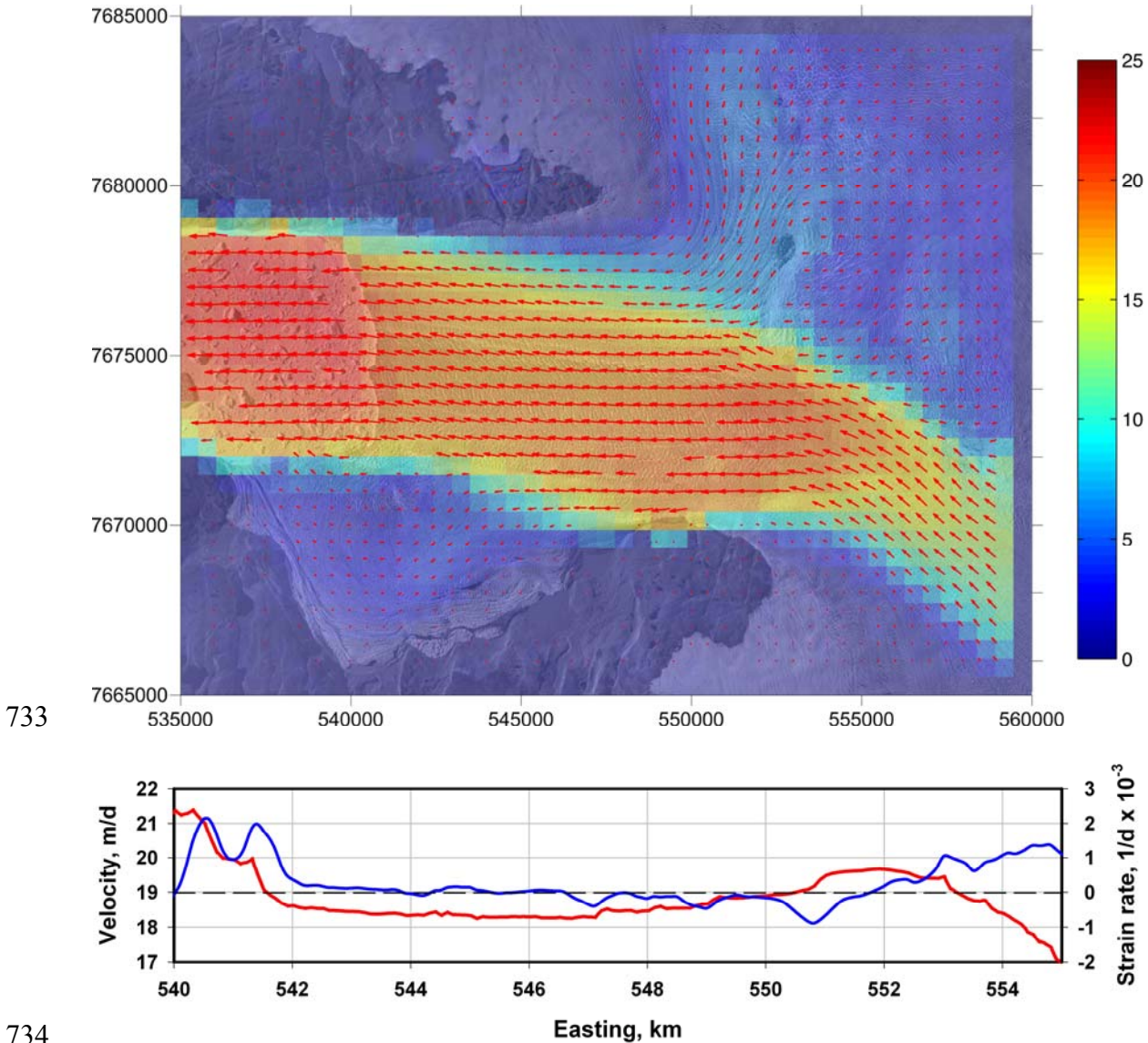
Figure 1. Landsat image showing the terminus of Jakobshavn Isbrae and Kangia Ice Fjord on 11-July-99. Black line shows terminus in 1985. Star is approximate location of CTD station 26 for data in Fig. 7.



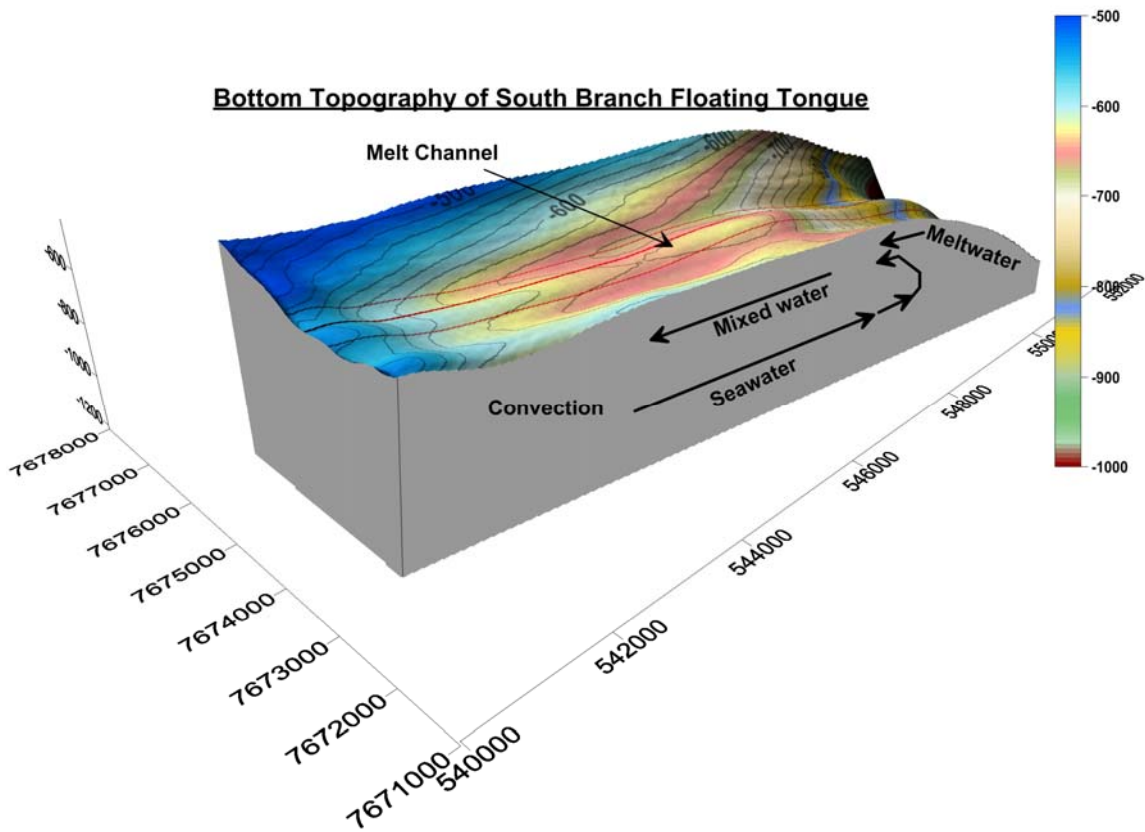
724
725
726
727
728

Figure 2. Shaded relief image of floating ice tongue and ice streams derived from July 24, 1985 photogrammetry (UTM zone 22N). Contour intervals (red) are 50 m (HAE). Dashed blue box outlines flow band analyzed for ice divergence and fluxes (Table 1;

729 *Figs. 3 and 4). Center flowlines for SB are shown in blue. 2007 terminus is from SPOT5*
 730 *imagery. Cyan circles are depth soundings (m) from Holland et al. (2008).*
 731
 732

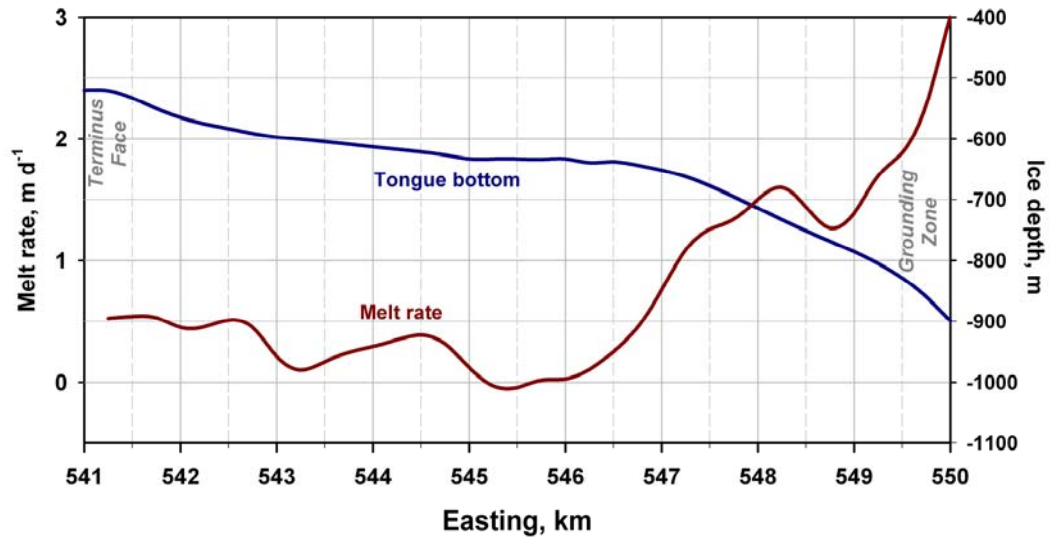


736 *Figure 3. a) Velocity map of Jakobshavn Isbrae terminus derived from feature tracking,*
 737 *using July 10 and July 24 orthophotos. b) Velocity (red) and strain rates (blue) along*
 738 *centerline of SB. Much of the SB floating tongue moves at speeds of about 18.5 m d⁻¹.*
 739



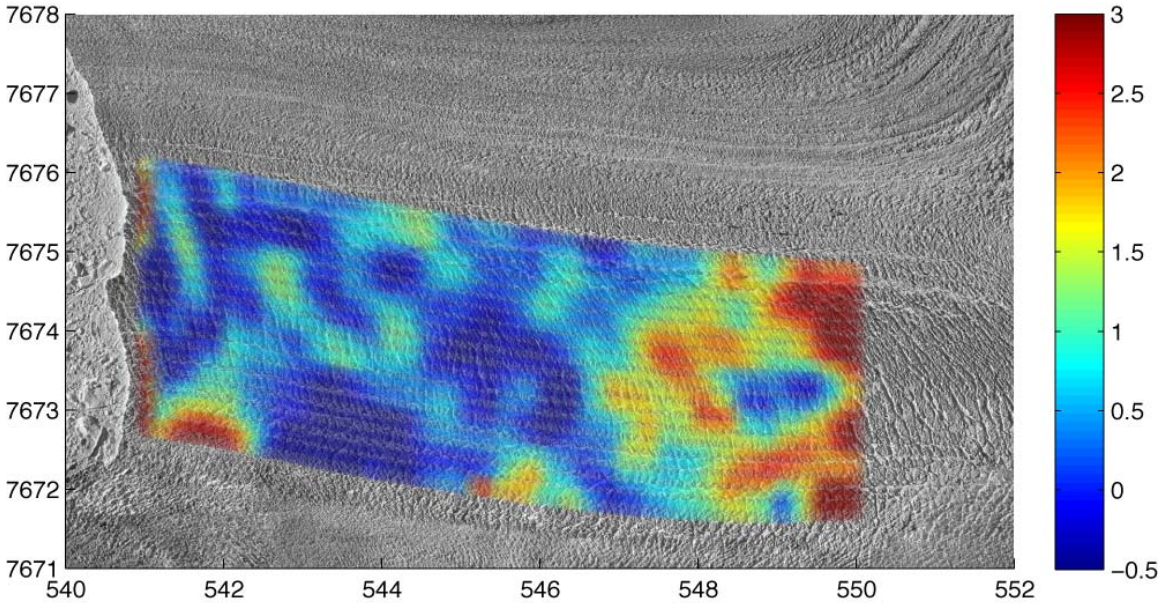
740
741
742
743
744
745
746
747
748

Figure 4. Bottom topography of a 10 km long, 3 km wide flow band of the south branch ice tongue derived by assuming hydrostatic equilibrium. Red lines are flowlines. Contour interval = 20 m.



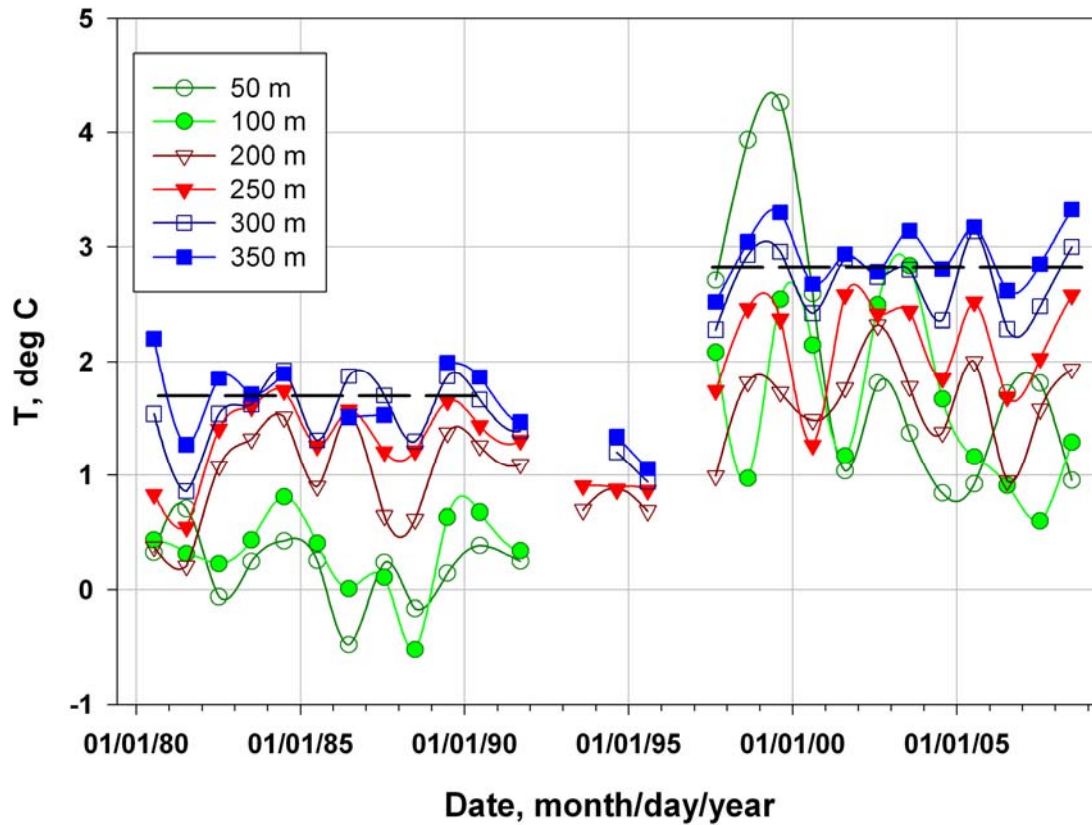
749
750
751
752
753
754
755

Figure 5. Width-averaged melt rates along the bottom of the SB floating ice tongue in 1985. Width-averaged depths of ice tongue with respect to sea level also shown.



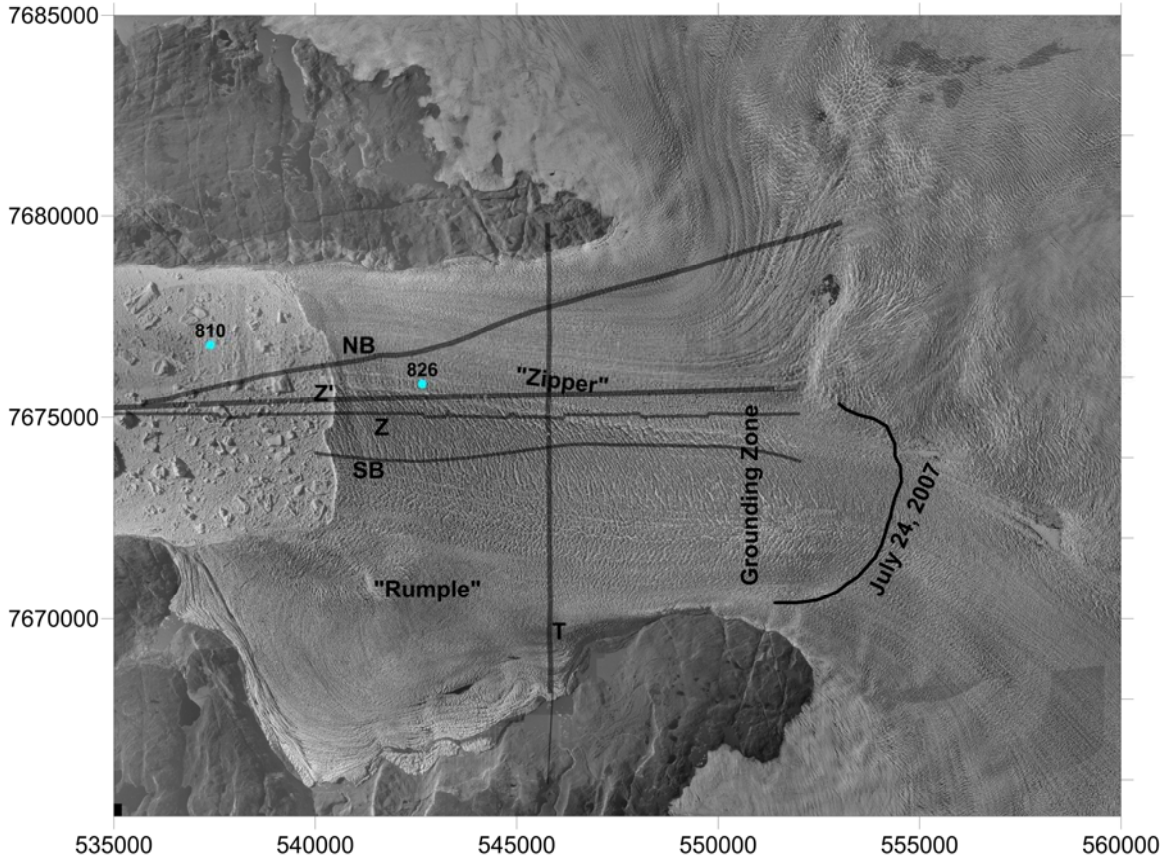
756
757
758
759
760
761

Figure 6. Map (km, UTM) showing distribution of bottom melting along the floating tongue in 1985. Analyses are along streamlines. Details much less than 0.5 km are lost because of the smoothing process used in constructing bottom topography.



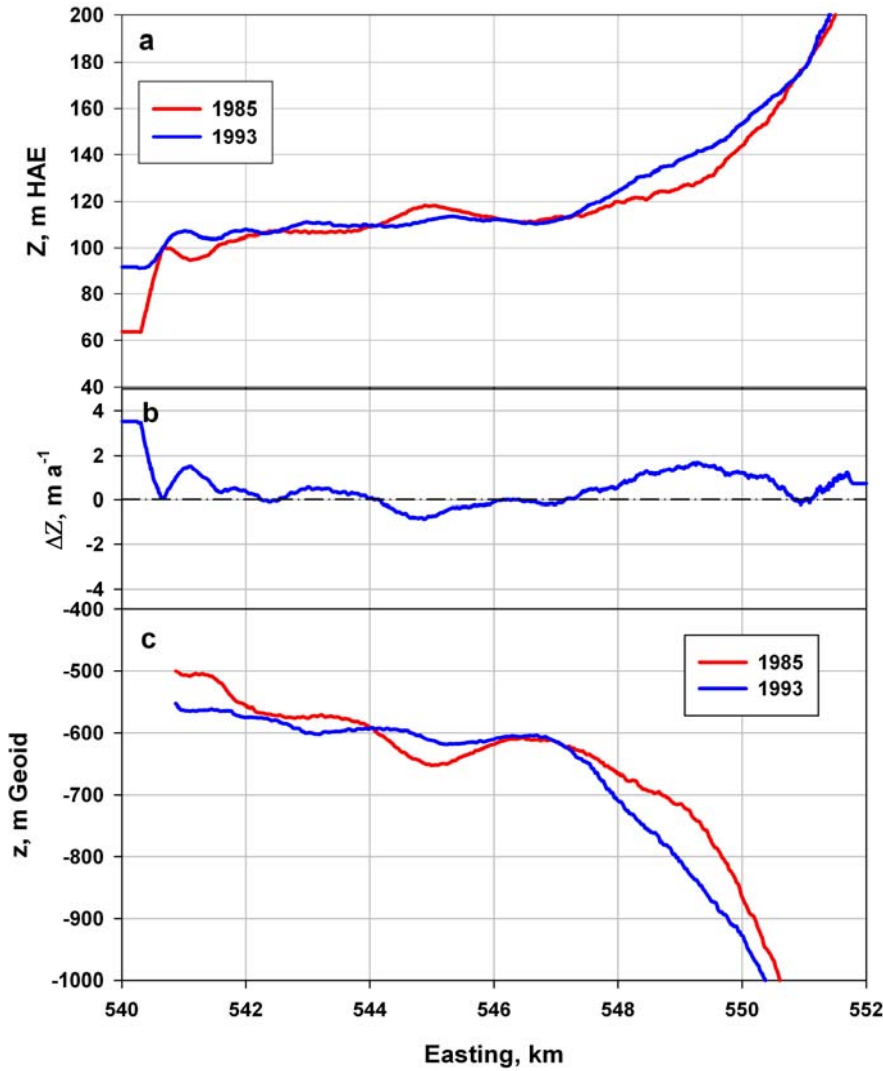
762
763
764
765
766
767
768
769
770

Figure 7. Summer seawater temperatures at various depths in Disko Bay at Station 26 near fjord entrance. Although there are data gaps for 1992 and 1996, there appears to have been a cooling trend during the mid-90's . Temperatures increased at all depth by 1997. Dashed lines indicate averaged temperature for depths of 300 – 350 m for 1980 – 1991 and 1997 - 2008.



771
772

773 *Figure 8. NASA ATM flight lines overlain on orthophoto of July 24, 1985 terminus (UTM*
774 *zone 22N). Line labels are keyed to Figures 9 -12. Cyan dots are water depths (m) from*
775 *Holland et al. (2008).*



776

777

778 *Figure 9. Surface profiles (a), change in elevation (b), and bottom profile (c) along 1993*

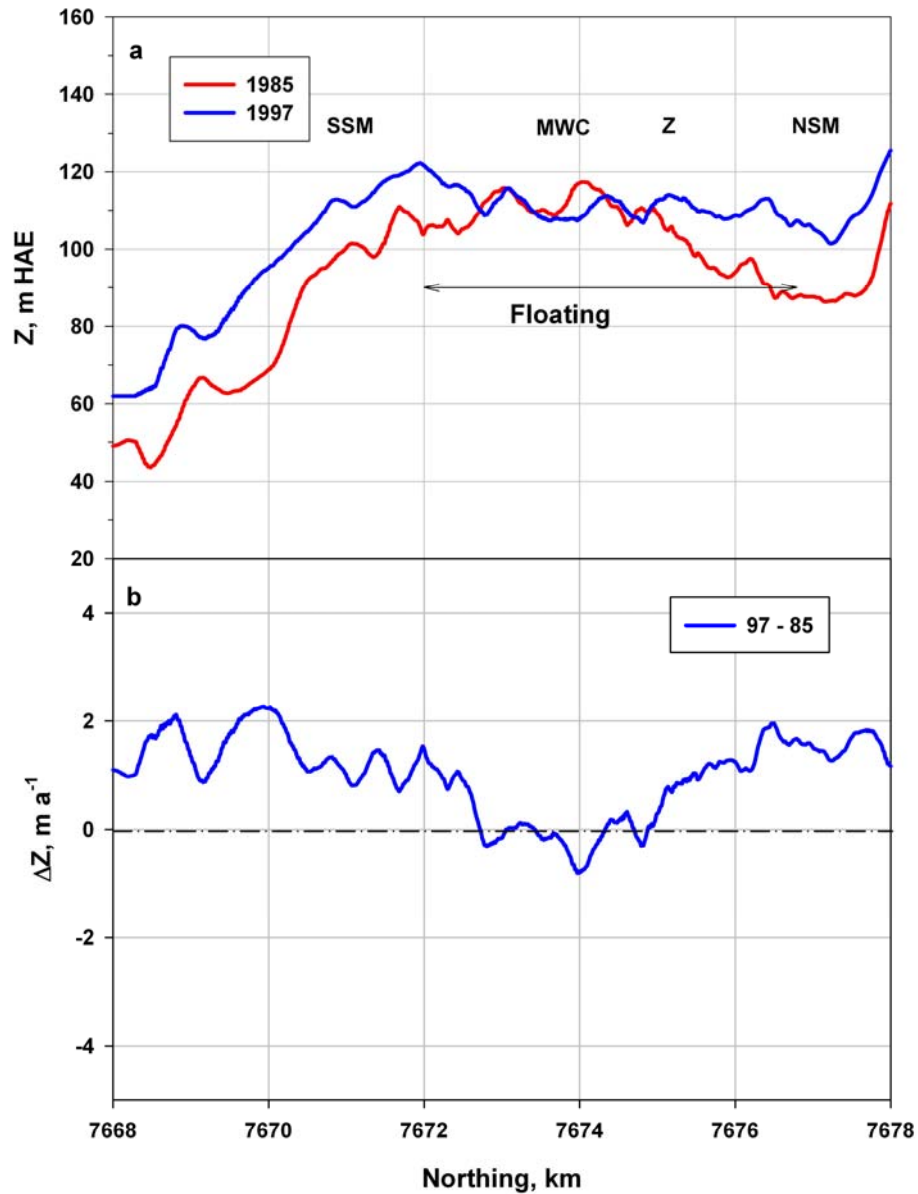
779 *ATM line SB between July 24, 1985 and July 9, 1993 (Fig. 8). The bottom profiles (c)*

780 *were calculated assuming hydrostatic equilibrium. The similarity in profiles lends*

781 *validity to our assumption that terminus geometry was relatively stable during this period*

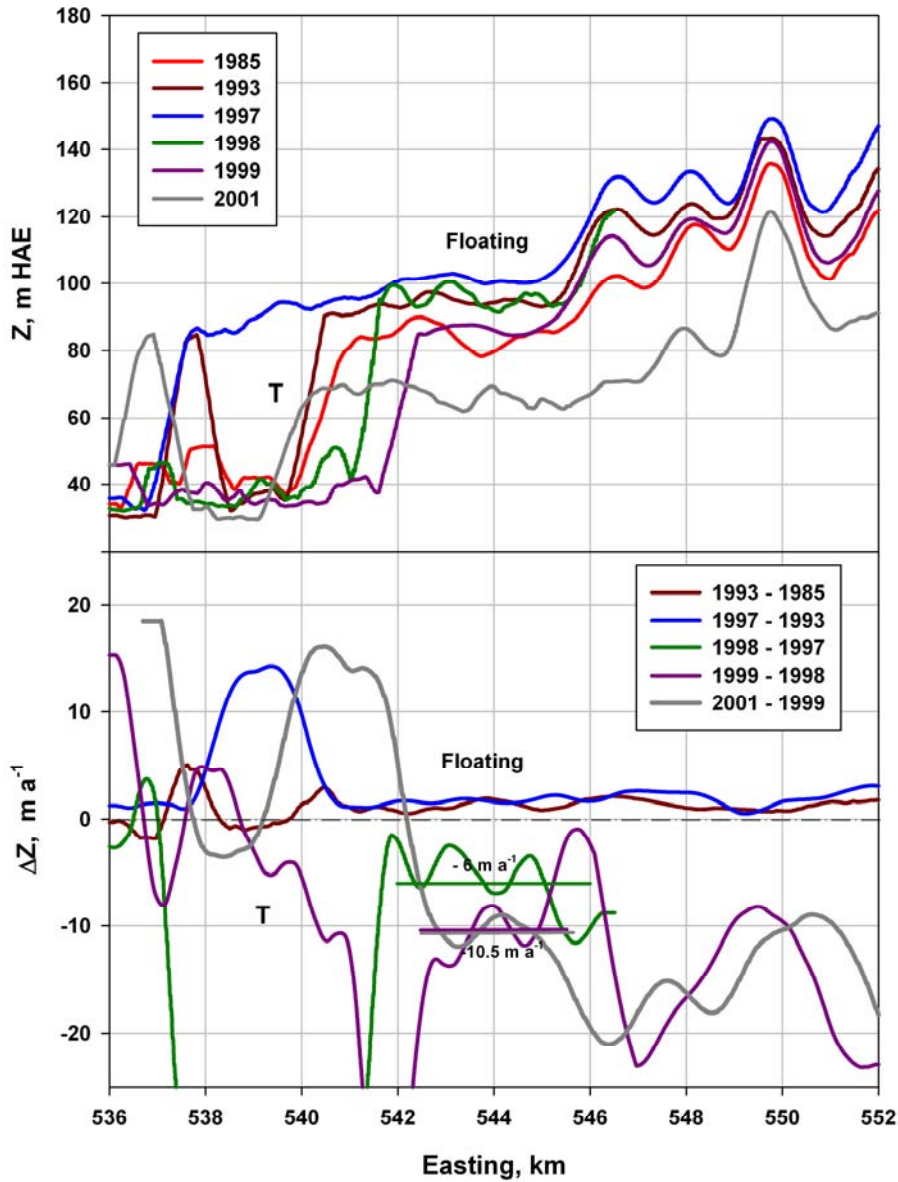
782 *although the GZ appears to have migrated down-channel by about 0.5 km.*

783



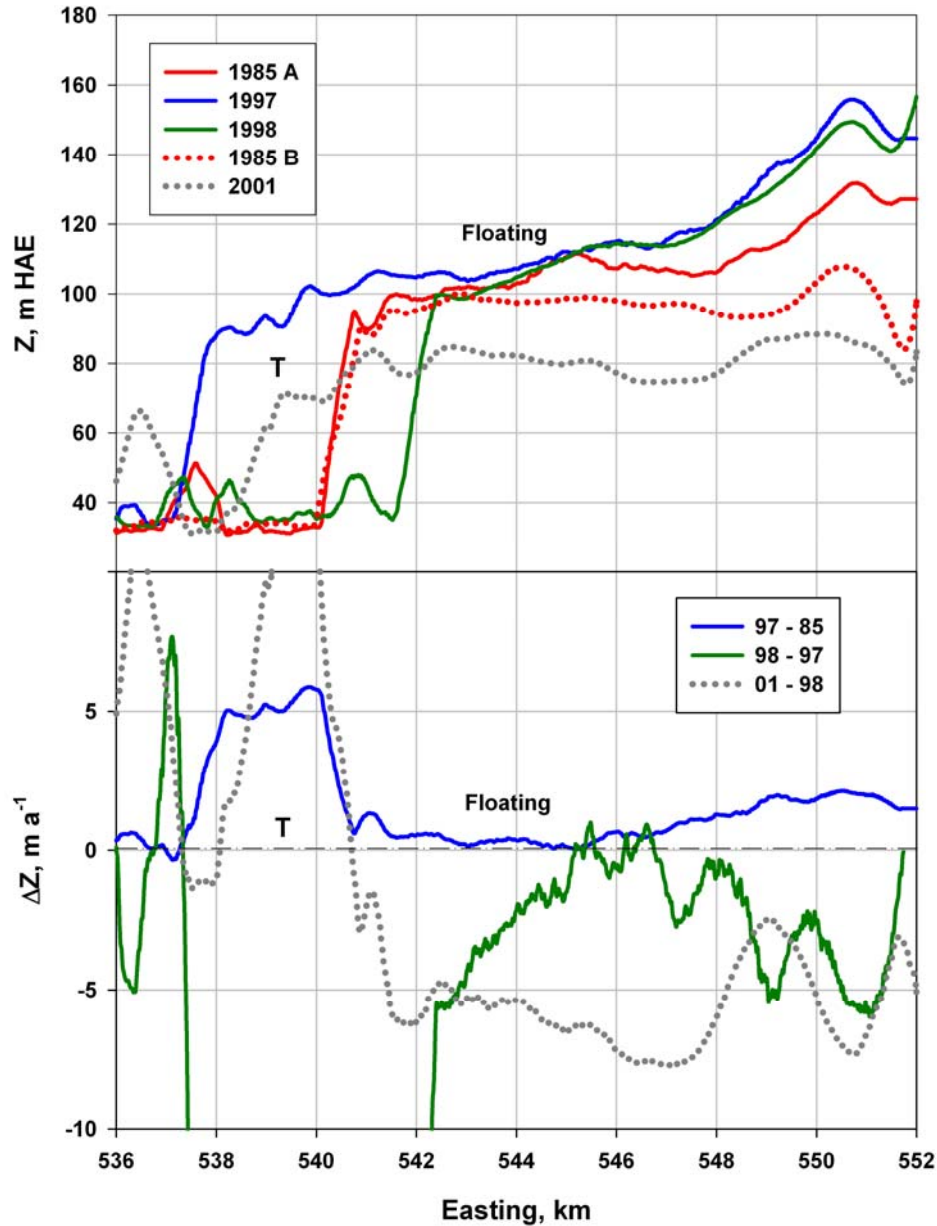
784
785

786 *Figure 10. ATM transverse profile “T” (Fig. 8) compared to 1985. SSM, MWC, and*
 787 *NSM locate the south wall shear margin, the “meltwater channel”, and the north wall*
 788 *shear margin, respectively. Thickening of ice is evident on either side of the SB flow*
 789 *band but not over the flow band itself*



790
791
792
793
794
795
796
797
798
799
800

Figure 11. Surface profiles (a) and change in elevation per year (b) for ATM line NB (Fig. 8). “T” marks the area where terminus fluctuations occur along this line: the terminus gradually advanced until 1997, then retreated 2 km by 1998 only to readvance again in 2001. The terminus along line NB was afloat to about 546 km Easting. This portion of the tongue gradually thickened between 1985 and 1997 as evidenced by a rise in free-board of $\sim 2 \text{ m a}^{-1}$. Rapid thinning was underway by 1998: the average change in surface elevation of -6 to -10 m a^{-1} between 1998 and 2001 corresponds to a rate of thinning of 60 to 100 m a^{-1} .



801
802
803
804
805
806
807
808

Figure 12. ATM profiles Z (solid) and Z' (dashed) flown over the terminus (Fig. 8). Changes in freeboard between 1997 and 1998 and in subsequent years are in good agreement with thinning of floating ice by disequilibrium bottom melting.